Supplementary Information

Enamel-inspired composite with robust mechanical properties and self-healing capability

Xin Guo[1,3], Chen Cui[1,3], Kai-Xin Li[1], Ze-Yong Zhuang[1], Meng-Han Zhu[1], Fu-Xing Zhao[1], Jing-Tong Ye[1], Qian-Hao Pan[1], Yu-Tao Wang[1], Chen Chen[1], Zong-Ying Huang[1], Mei-Hua Wang[1], Xiao-Jing Qiu[1], Bang Yu[1], Li-Wen Zhang[1], Jing-Long Wang[1], Zhen He[1*], and Shu-Hong Yu[1,2*]

[1]*Shenzhen Key Laboratory of Sustainable Biomimetic Materials, Guangdong Provincial Key Laboratory of Sustainable Biomimetic Materials and Green Energy, Department of Materials Science and Engineering, Institute of Innovative Materials, Guangming Advanced Research Institute, Southern University of Science and Technology, Shenzhen 518055, China.*

[2]*New Cornerstone Science Laboratory, Division of Nanomaterials & Chemistry Hefei National Research Center for Physical Sciences at the Microscale, Department of Chemistry, Institute of Biomimetic Materials & Chemistry, Anhui Engineering Laboratory of Biomimetic Materials, University of Science and Technology of China, Hefei 230026, China.*

[3]*These authors contributed equally to this work.*

[*] Correspondence and requests for materials should be addressed to the author: Zhen He (hez@sustech.edu.cn) or Shu-Hong Yu (yush@sustech.edu.cn).

Supplementary Materials

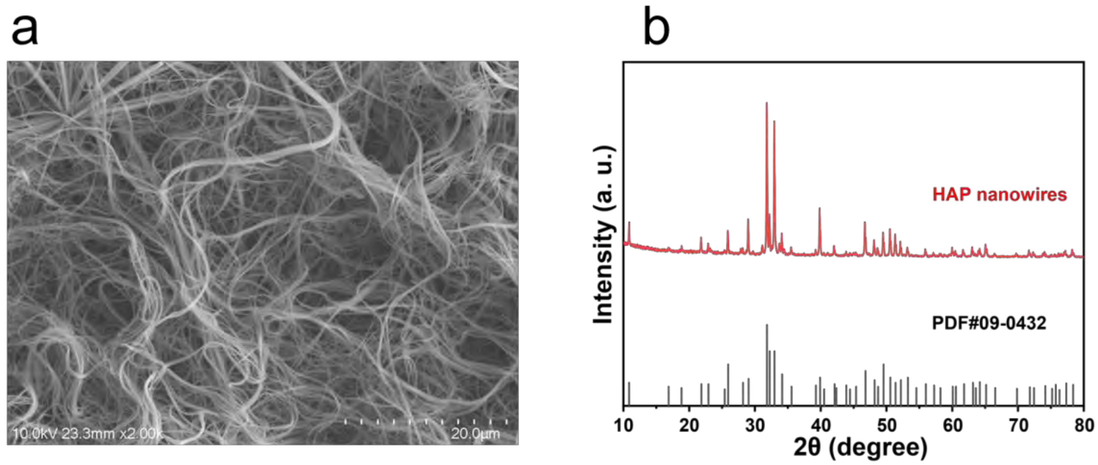

Supplementary Fig. 1 | Fabrication of HAP NWs. a, SEM image of HAP NWs. **b,** XRD pattern of HAP NWs.

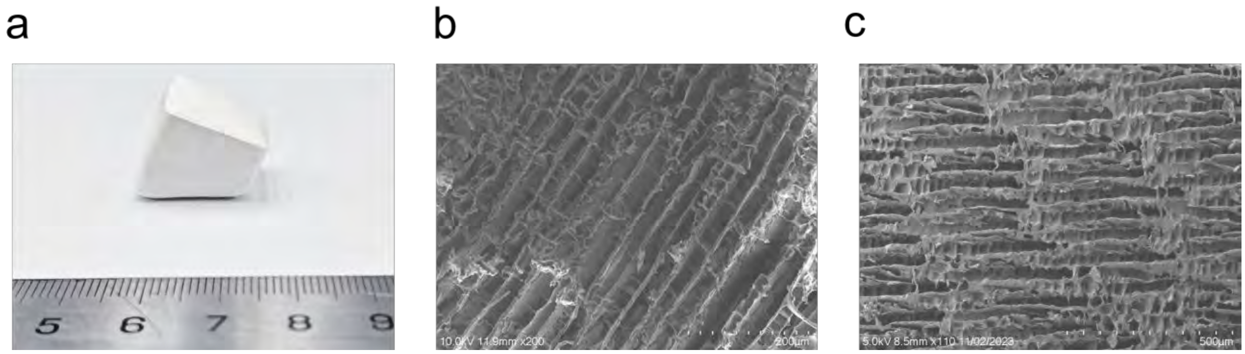

Supplementary Fig. 2 | Image of lamellar HAP with different ratios of PVA to HAP. a, Photograph of the lamellar HAP. **b,c,** The cross-section SEM images of the lamellar HAP scaffold with different ratios of PVA to HAP (**b**) PHB-5, (**c**) PHB-15.

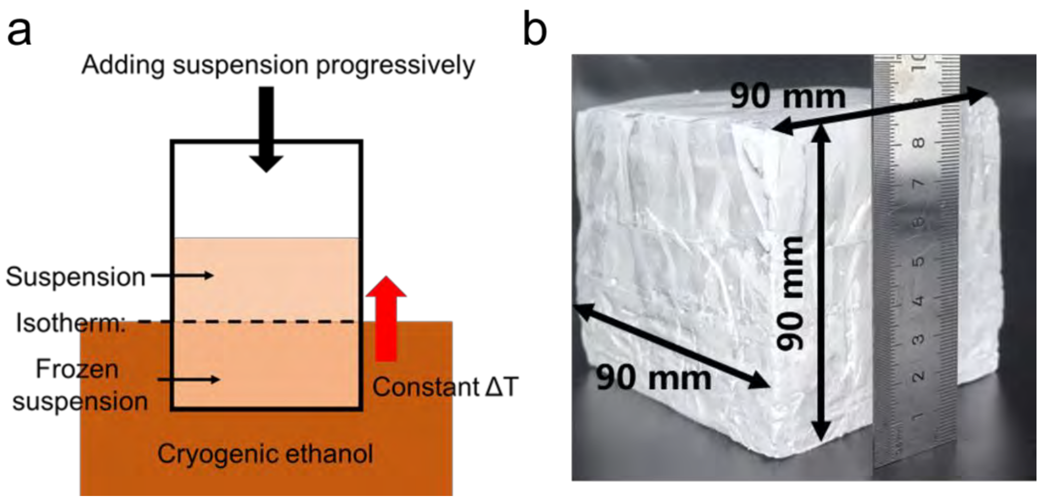

Supplementary Fig. 3 | a, Scheme of scalable fabrication and optical image of a large-sized lamellar scaffold. **b,** Photograph of the lamellar HAP scaffold.

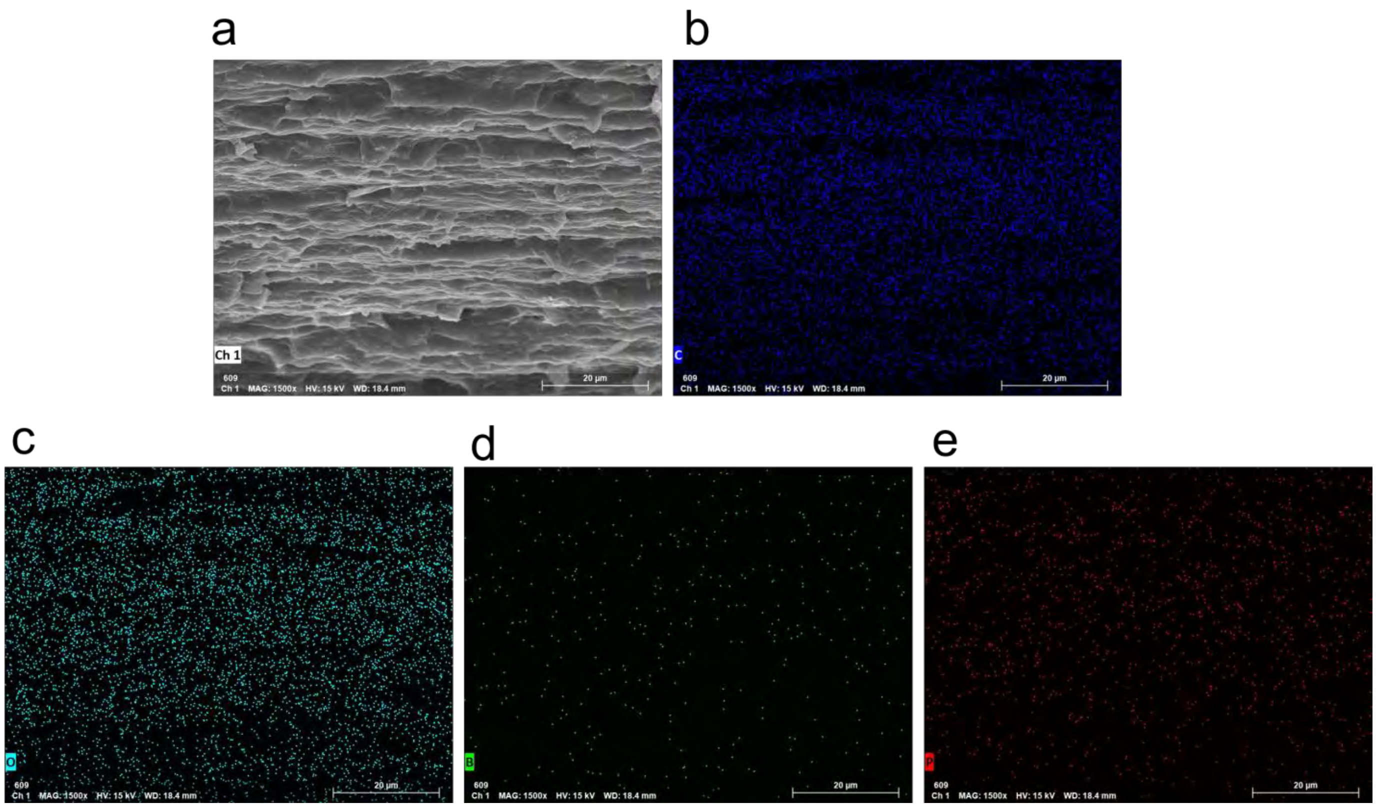

Supplementary Fig. 4 | Elemental composition of PHB. a, SEM image of the cross-section of PHB. **b-e,** corresponding EDS mapping (with detected elements of C, O, B and P) of the PHB nanocomposite.

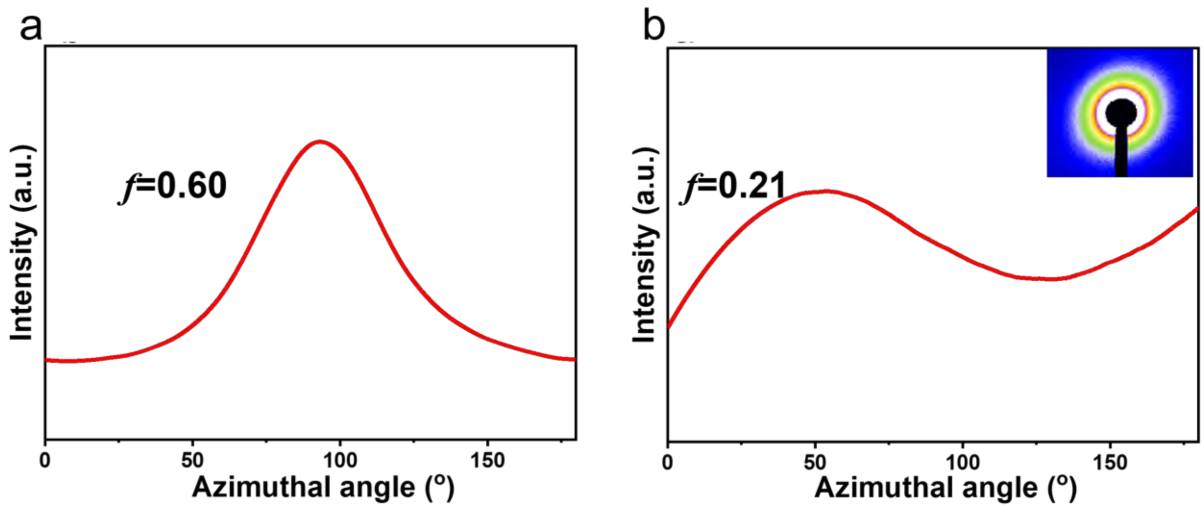

Supplementary Fig. 5 | Orientation characterization. a,b, Azimuthal angle (φ) plots of PHB-10 (**a**) and PHB-R (**b**), f represents the Herman's orientation factors, inset is 2D SAXS image of PHB-R.

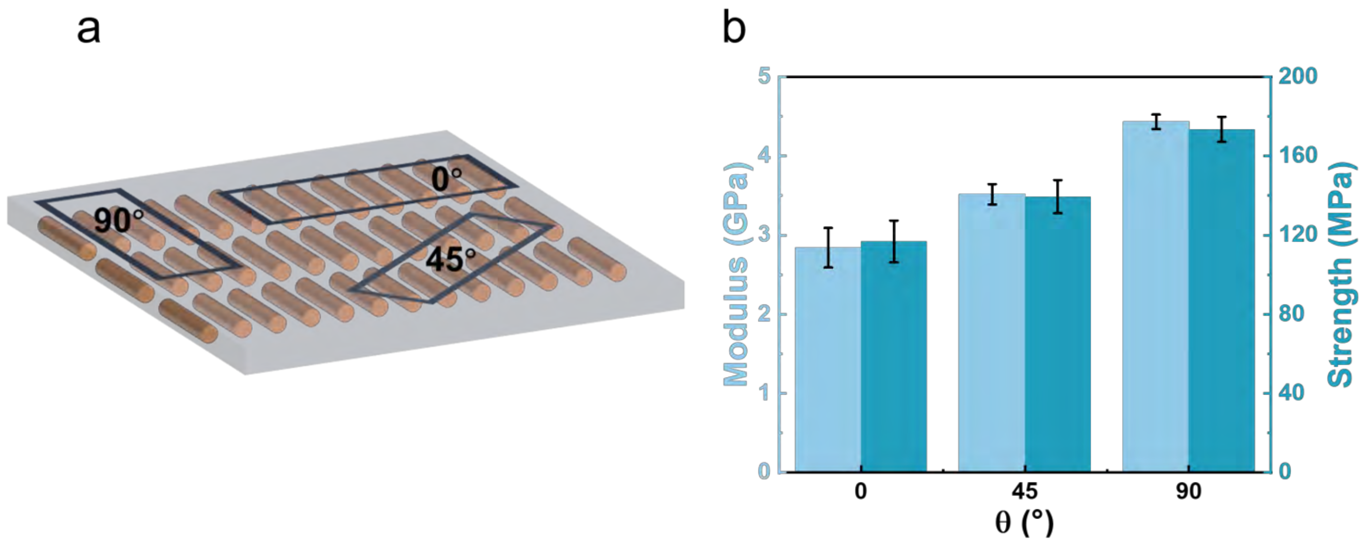

Supplementary Fig. 6 | a, Schematic diagram of three-point bending tests of different load directions. **b,** Comparison of mechanical properties of PHB composites with different load directions.

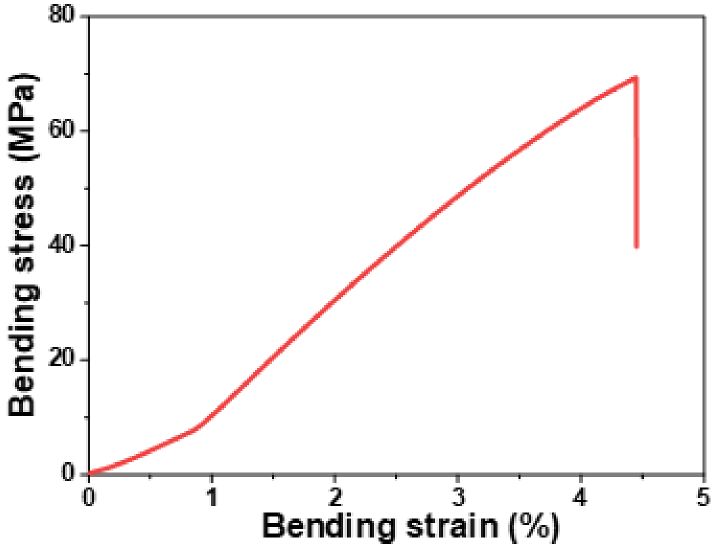

Supplementary Fig. 7 | The flexural stress-strain curves of pure PVA.

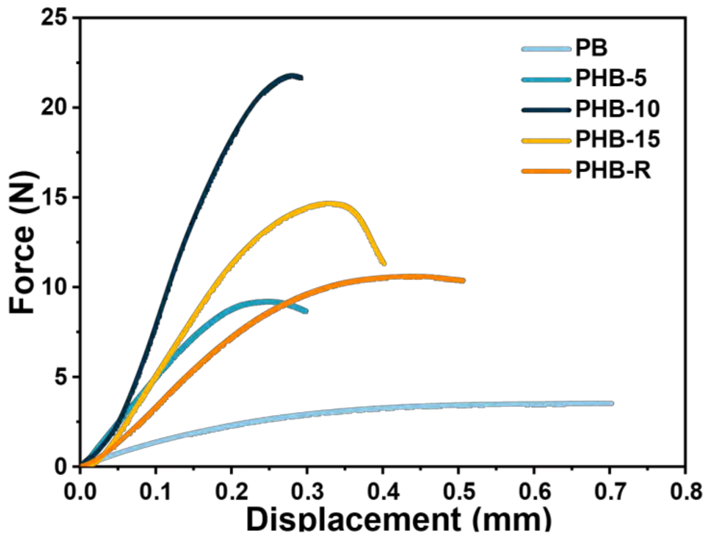

Supplementary Fig. 8 | Force-displacement curves of PB, PHB-R, and PHB composites with different HAP NWs contents.

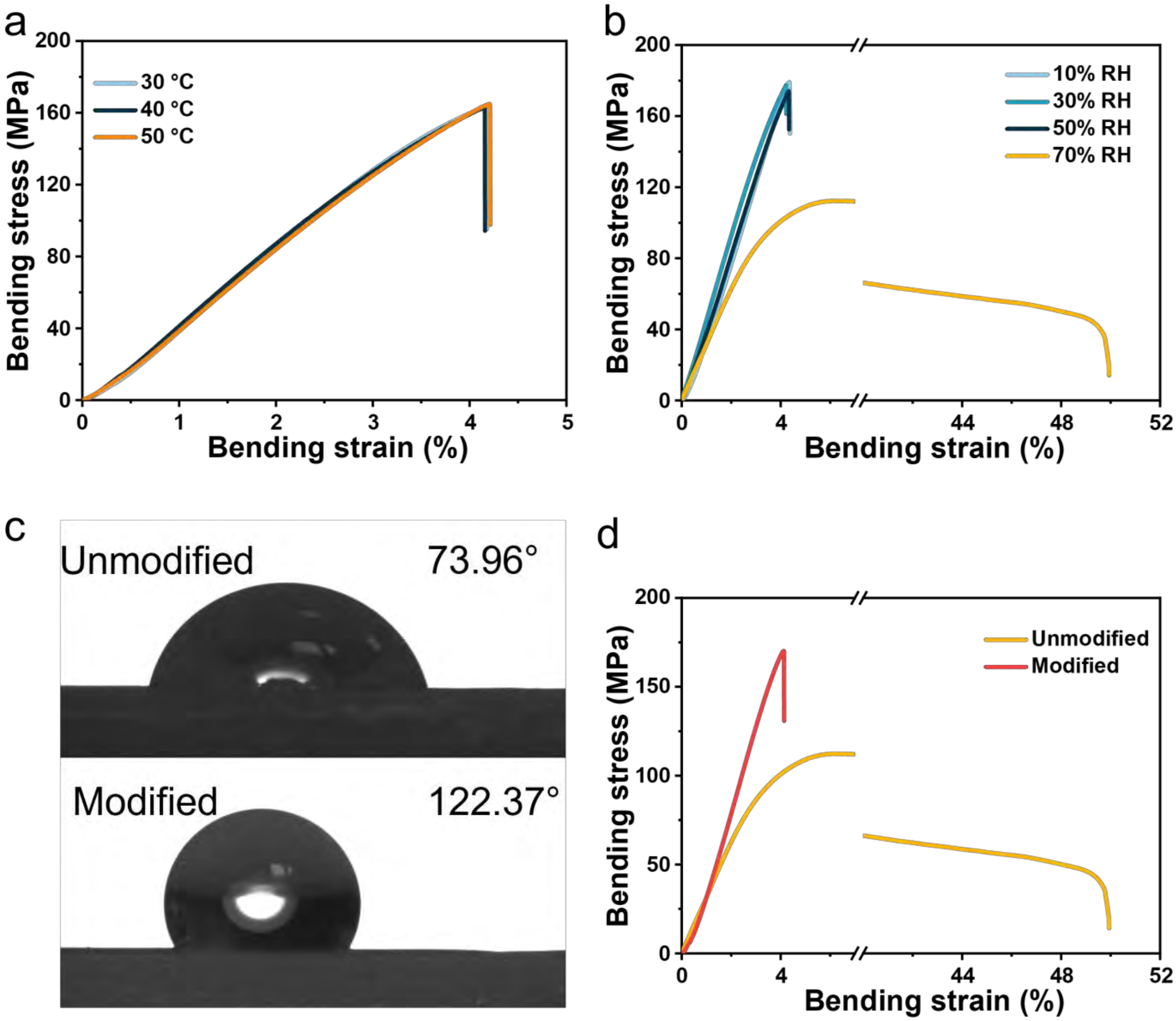

Supplementary Fig. 9 | a, Flexural stress-strain curves of PHB composites with different temperatures (30-50 °C). **b,** Flexural stress-strain curves of PHB composites at room temperature with different relative humidity (10%-70% RH). **c,** Contact angle of unmodified and modified PHB composites. **d,** Flexural stress-strain curves of unmodified and modified PHB composites.

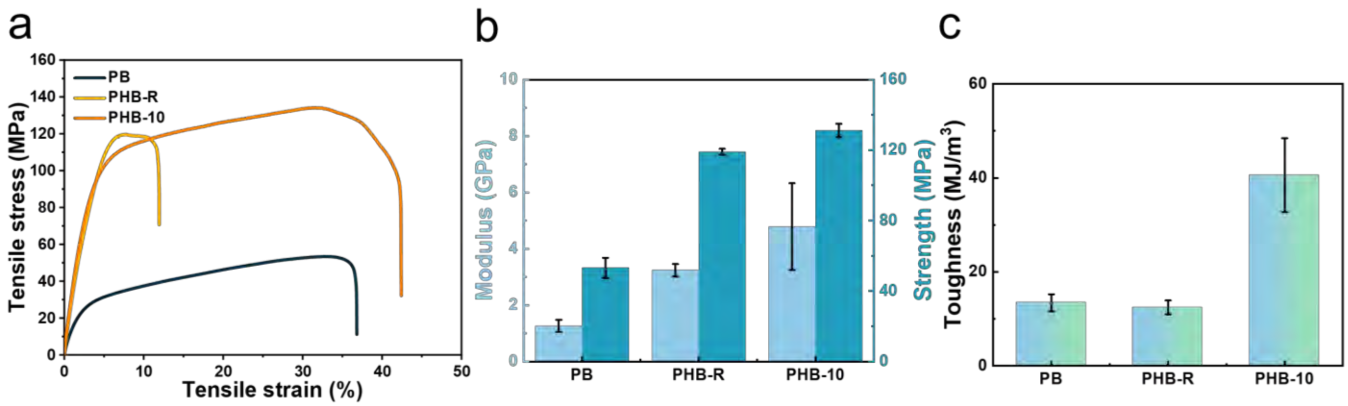

Supplementary Fig. 10 | a, Tensile stress-strain curves of the PB, PHB-R, and PHB-10 composites. **b,c,** Comparison of (**b**) flexural stress, modulus and (**c**) toughness of the PB, PHB-R, and PHB-10 composites.

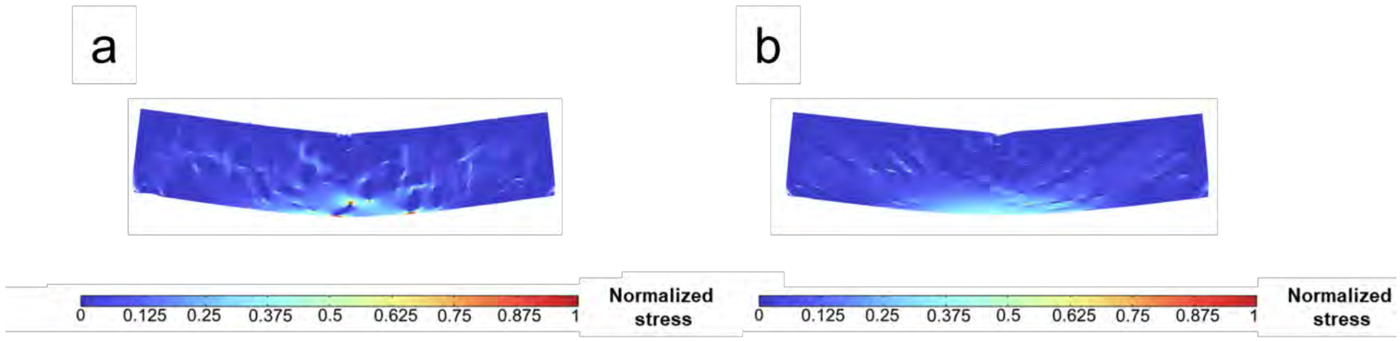

Supplementary Fig. 11 | a,b, 2D FEM simulations of composite with (**a**) disordered HAP NWs and (**b**) ordered HAP NWs for the three-point bending test. Based on identical interface interaction for PHB-10 and PHB-R, the microstructure has a significant role in the improvements in mechanical properties. In contrast to the random distribution of HAP, the ordered arrangement of HAP in PHB-10 like enamel ensures a better transfer of stress to avoid catastrophic damage thus enhancing the mechanical properties.

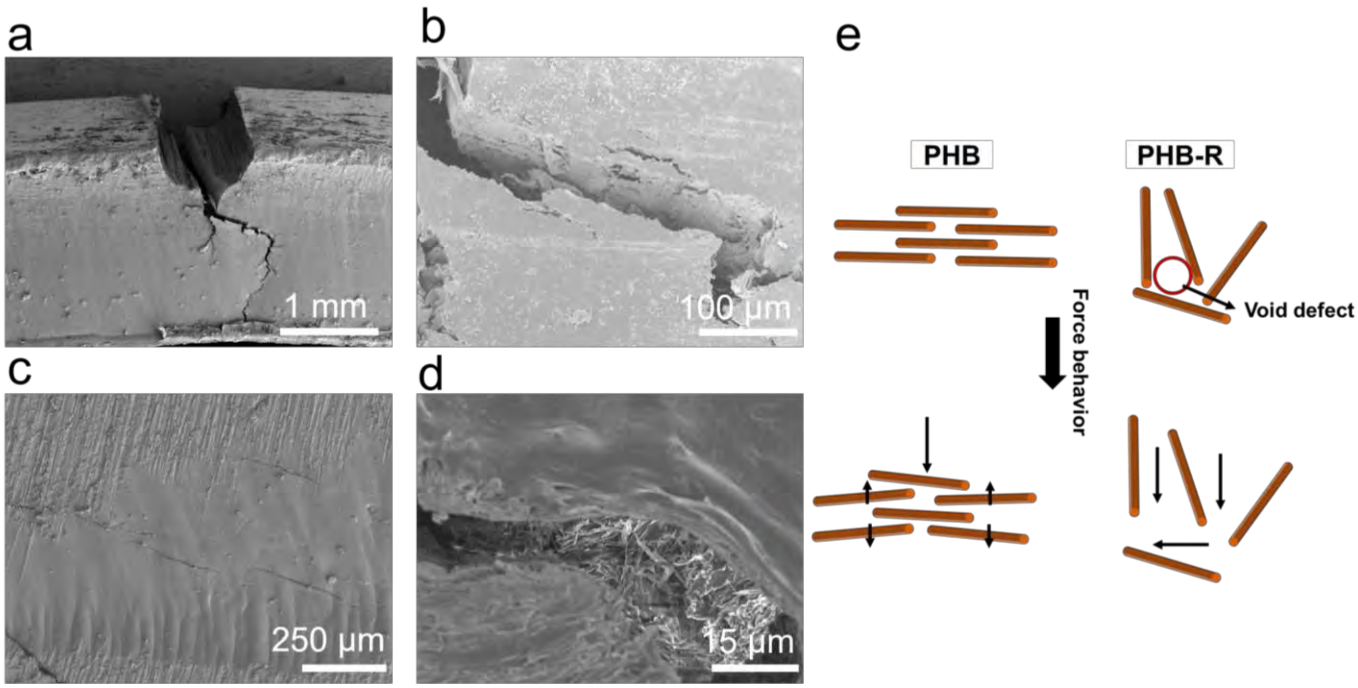

Supplementary Fig. 12 │ Mechanism analysis of the fracture process of the PHB-R composites. a, SEM image of the PHB-R composites showing the crack deflection extension. **b,** SEM image of crack branching. **c,** SEM image of pull-out of nanowires and nanowires bridging. **d,** SEM image of cracks away from the main crack. **e,** Schematic illustrations of the stress behavior of the PHB and PHB-R composites.

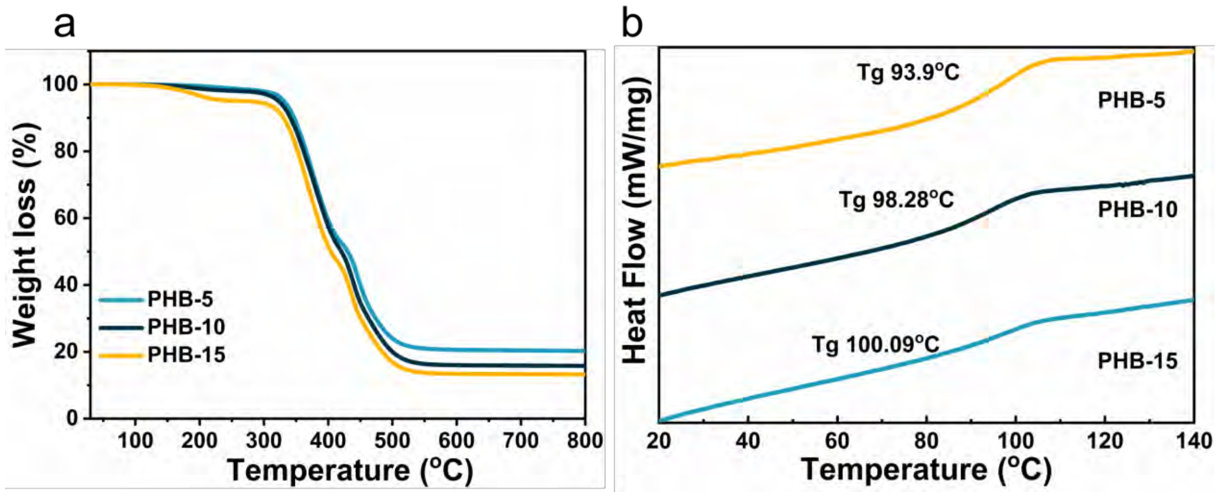

Supplementary Fig. 13 | Thermal behaviours of PHB composites. a, TG curves of PHB composites. **b,** DSC curves of PHB composites.

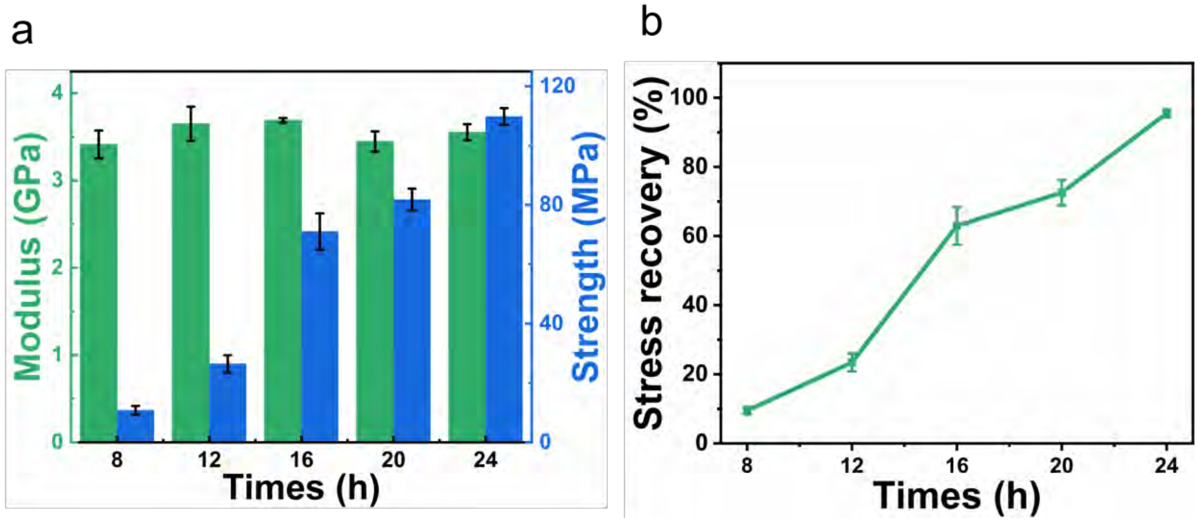

Supplementary Fig. 14 │ Healable performance of the PB. a, Modulus and strength of healed PB at different times. **b,** self-healing efficiency of healed PB at different times.

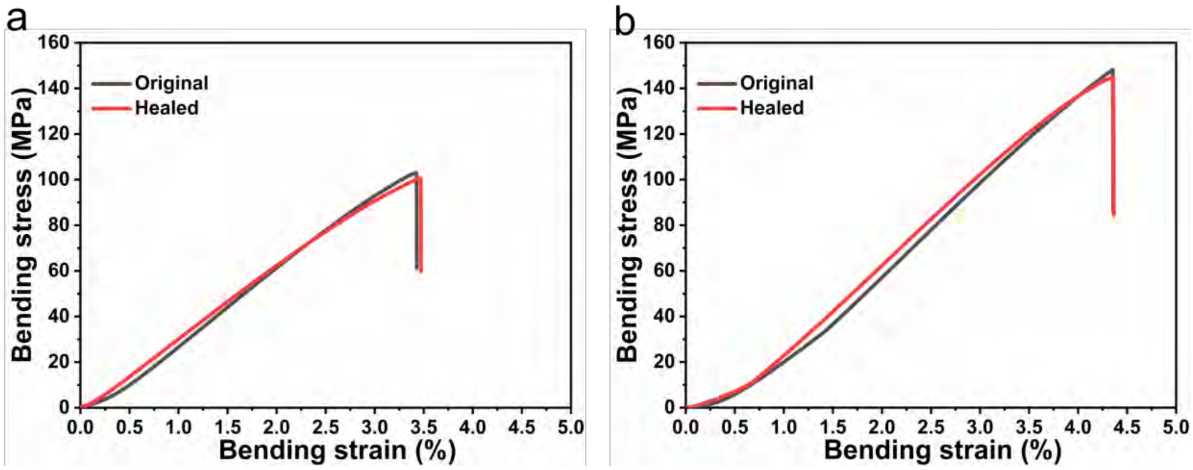

Supplementary Fig. 15 | Healable performance of the PHB composites. a,b, The flexural stress-strain curves of (**a**) healed PHB-5 and (**b**) healed PHB-15 after 24 h at 80 °C.

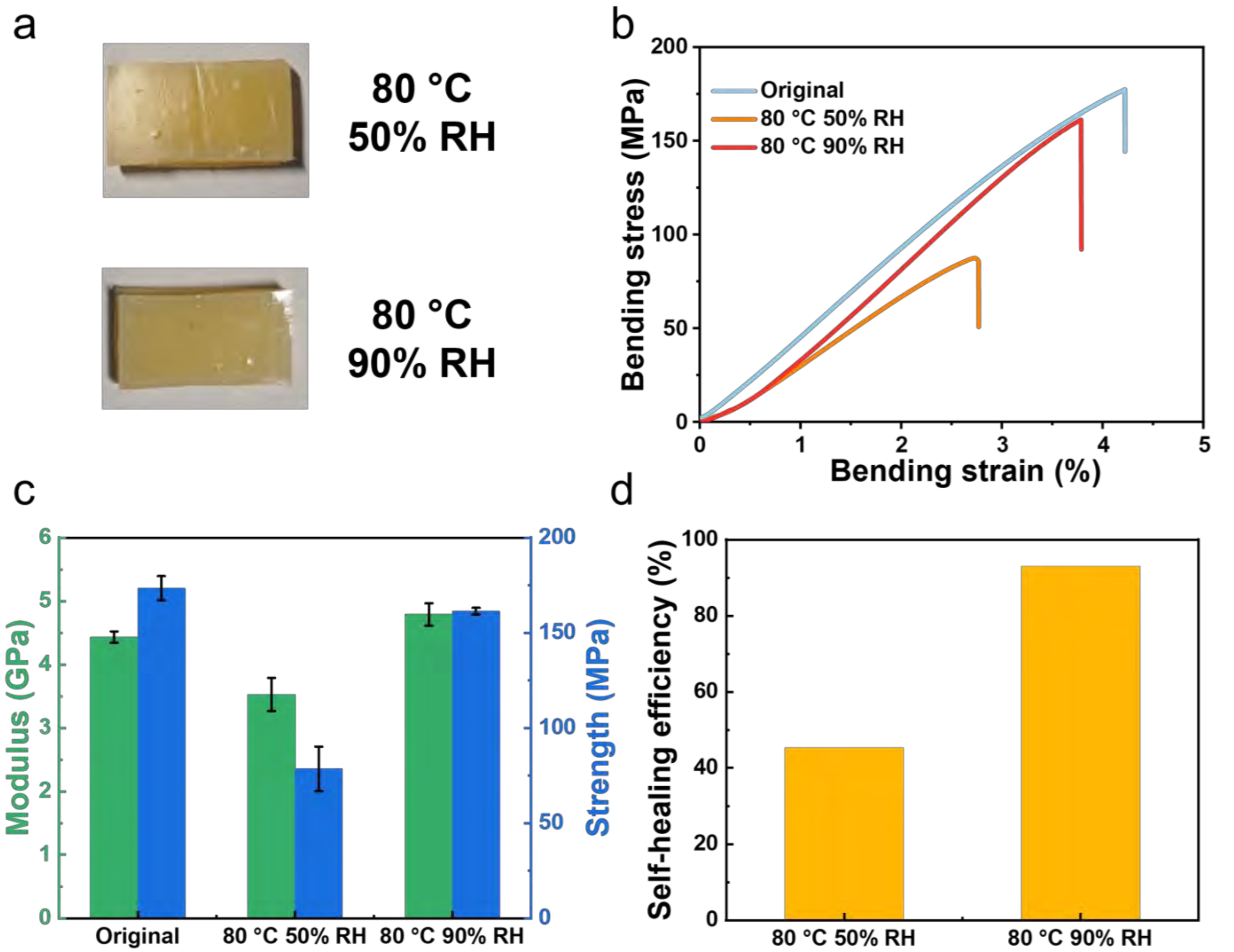

Supplementary Fig. 16 | a, Photographs of PHB composites spline healing at 80 °C, 50% RH and 80 °C, 90% RH for 24 h, respectively. **b,** Flexural stress-strain curves of PHB composites spline healing at 80 °C, 50% RH and 80 °C, 90%. **c, d,** Comparison of (**c**) flexural strength, modulus and (**d**) self-healing efficiency of PHB composites spline healing at 80 °C, 50% RH and 80 °C, 90% RH.

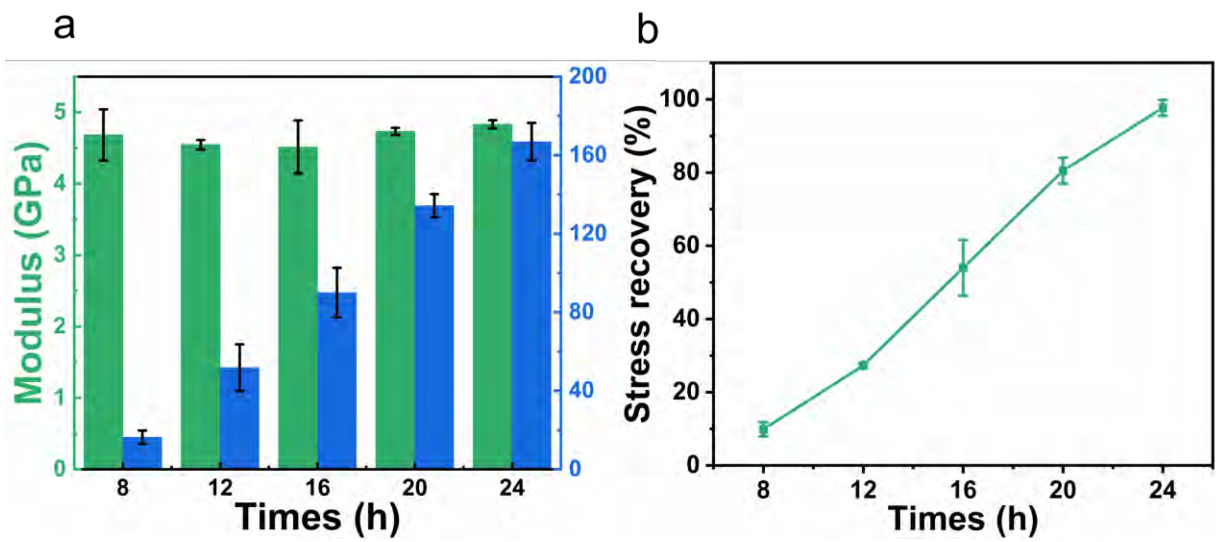

Supplementary Fig. 17 | Healable performance of the PHB-10. a, Modulus and strength of healed PHB-10 at different times. **b,** Self-healing efficiency of healed PHB-10 at different times.

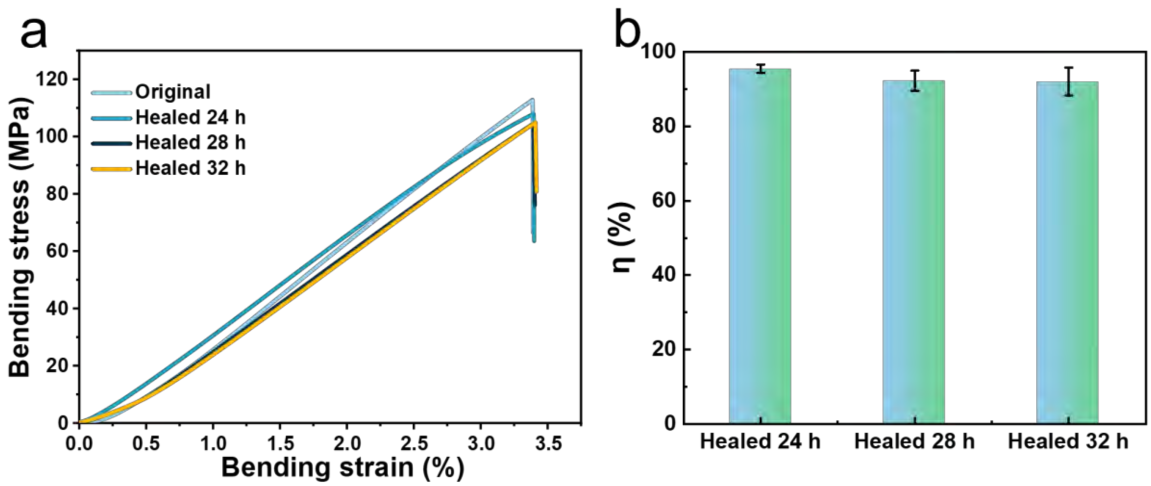

Supplementary Fig. 18 | a, The flexural stress-strain curves of PB composites with different healed times. **b,** Comparison of self-healing efficiency (η) of PB composites with different healed times.

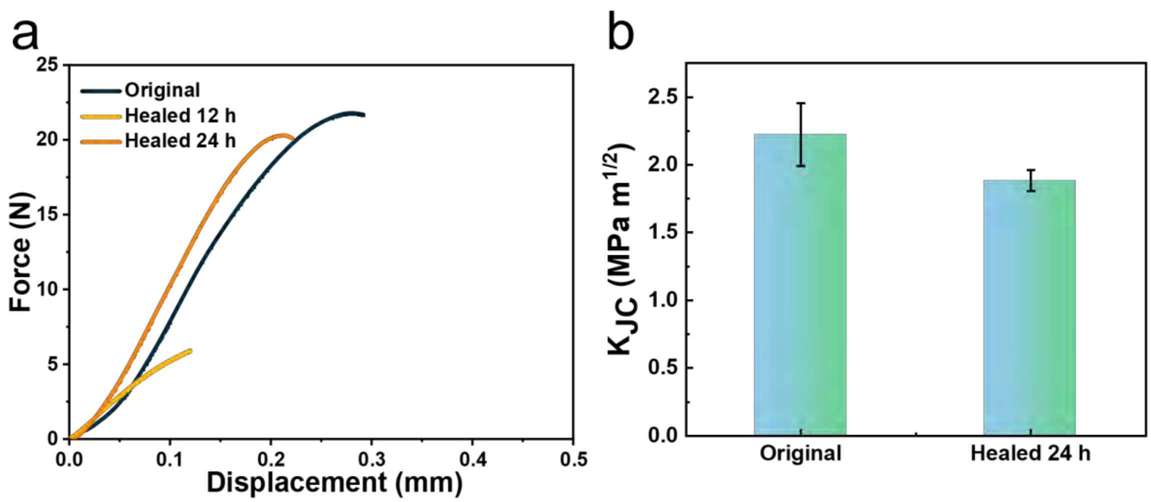

Supplementary Fig. 19 | a, Force-displacement curves of PHB-10 with different healed times. **b,** Comparison of fracture toughness of original and healed 24 h PHB.

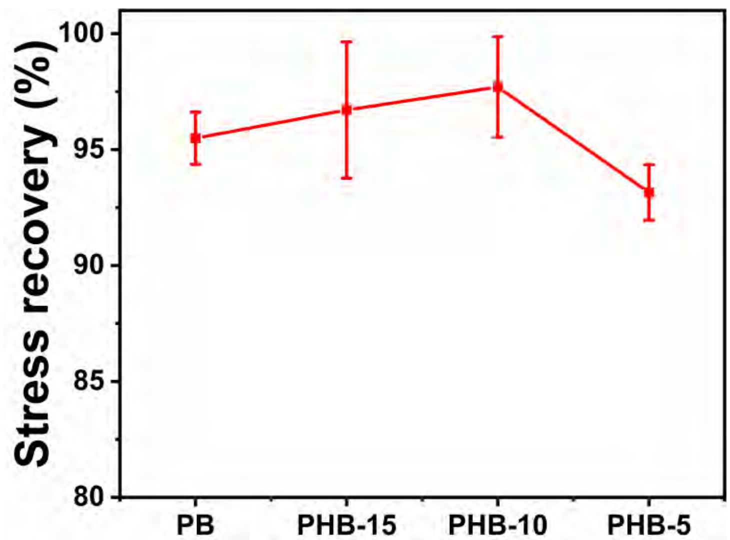

Supplementary Fig. 20 | Self-healing efficiency of PHB nanocomposites with different ratios of PVA to HAP NWs.

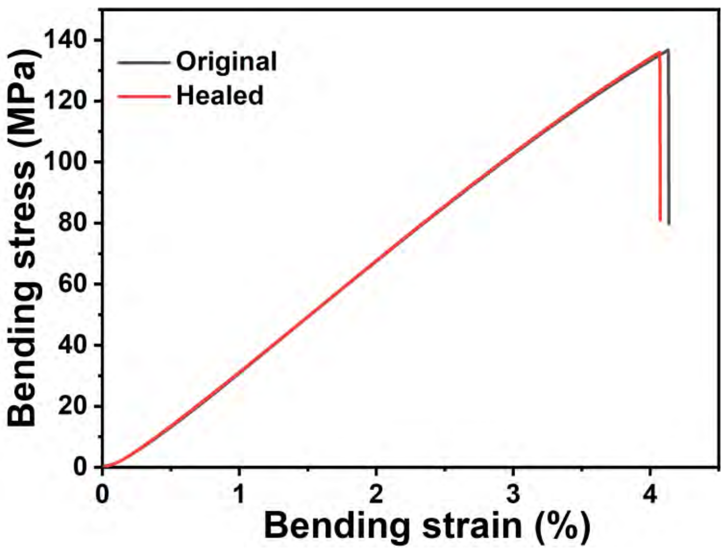

Supplementary Fig. 21 | The flexural stress-strain curves of healed PHB-R.

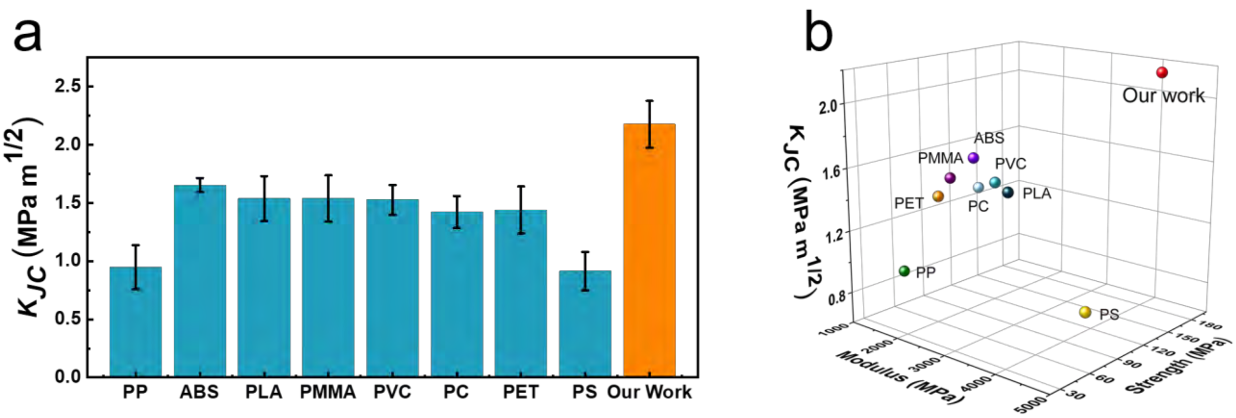

Supplementary Fig. 22 | a, Fracture toughness comparisons of the composites with engineering plastics. **b,** Ashby chart summarizing the strength vs. modulus vs. fracture toughness of engineering plastics.

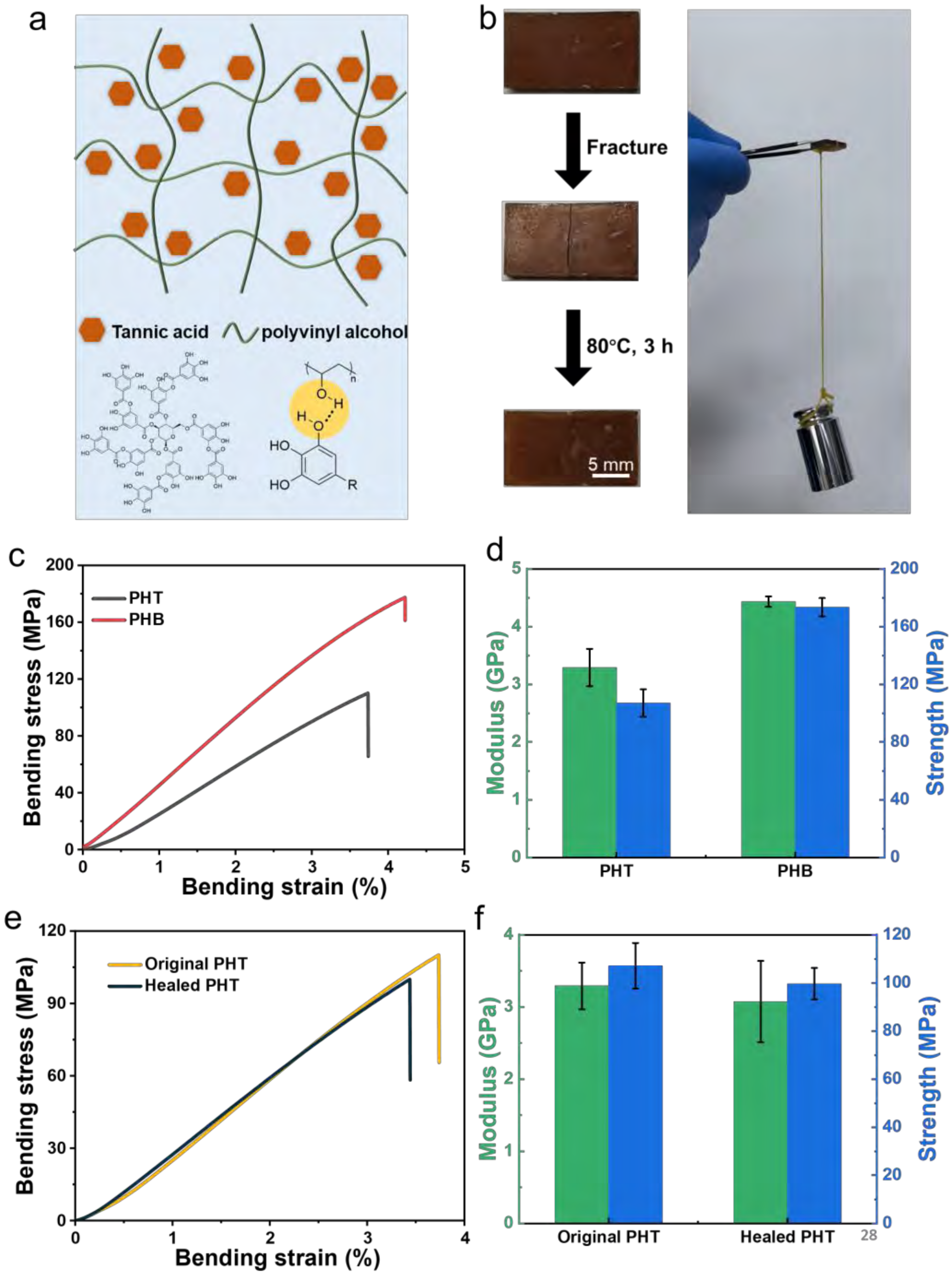

Supplementary Fig. 23 | a, Schematic illustration of the hydrogen bonded cross-linked network of tannic acid and polyvinyl alcohol. **b,** Photographs of the sample spline healing at 80 °C for 3 h. c. Flexural stress-strain curves of PHT and PHB composites. d. Comparison of flexural strength and modulus of the PHT and PHB composites. e. Flexural stress-strain curves of original PHT composites and healed PHT composites at 80 °C for 24 h. f. Comparison of flexural strength and modulus of original PHT composites and healed PHT composites at 80 °C for 24 h.

Supplementary Table 1 │ Summary of mechanical behavior of various self-healable materials.

	References	Species	Mechanism	Modulus (MPa)	Strength (MPa)	Healing Ratio (%)	Damaged manner	Healing Conditions
1	Adv. Mater. 35, 2300286 (2023).	Elastomer	Hydrogen bond	69.33	142.35	--	Fracture	50 °C, DMF, 24 h
2	Adv. Funct. Mater. 30, 1907109 (2020).	Elastomer	Hydrogen bond	1.95	4.83	--	Fracture	Room temperature, 48 h
3	Adv. Funct. Mater. 30, 1907139 (2020).	Elastomer	Host-guest interaction and hydrogen bond	0.51	1.05	93	Fracture	55 °C,48 h
4	Chem. Eng. J. 410, 128300 (2021).	Elastomer	Oxime-carbamate interaction and hydrogen bond	4.9	29.5	99.8	Fracture	70 °C, 12 h
5	Mater. Horiz. 8, 2238-2250 (2021).	Elastomer	Hydrogen bond	7.84	33.4	93	Fracture	Room temperature, DMF, 12 h
6	Angew. Chem. Int. Ed. 60, 26192 (2021).	Elastomer	Waals interactions	42.1	15.3	95	Fracture	25 °C, 120 h
7	Angew. Chem. Int. Ed. 62, e202305282 (2023).	Elastomer	Host-guest interaction and hydrogen bond	0.32	5.80	91	Fracture	Room temperature, 24 h
8	Adv. Mater. 31, 1904956 (2019).	Hydrogel	Imine bond and hydrogen bond	7.2	4.3	84	Fracture	Room temperature, 80 min
9	Chem. Mater. 30, 1729–1742 (2018).	Hydrogel	Host-guest interaction	0.093	0.18	--	Fracture	Room temperature
10	Natl. Sci. Rev. 9, nwab147 (2022).	Hydrogel	Hydrogen bond	0.029	1.02	--	Fracture	Room temperature, 60s
11	Angew. Chem. Int. Ed. 60, 7947 (2021).	Glass	Hydrogen bond	1560	15.99	99.1	Fracture	25 ℃ , 1 MPa, 1 h
12	Nat. Commun. 7, 10995 (2016).	Glass	Hydrogen bond	3040	6.42	--	Fracture	ultraviolet light, 5 min
13	Macromolecules 54, 1760–1766 (2021).	Resin	Borate ester bond	114	11	--	Fracture	160 ℃ , 2 MPa, 5 min
14	J. Mater. Chem. A, 9, 4055-4065 (2021).	Resin	Hydrogen bond	2840	100.12	94	Fracture	120 °C, DMF, 1 h

15	Macromolecules 53, 7914–7924 (2020).	Resin	Hydrogen bond	1740	68.5	99.7	Fracture	120 ℃ , DMF, 1 h
16	Nat. Commun. 10, 800 (2019).	Composite	Diels-Alder reaction	3600	62.2	95	Fatigue	50 ℃ , 24 h
17	Matter 4, 2474 (2021).	Composite	Hydrogen bond	6110	45.38	98	Scratch	Near-infrared light, 30 s
18	Our work	Composite	Borate ester bond	4430	173.47	97.7	Fracture	80 ℃ , 24 h

Supplementary Table 2 | Summary of mechanical behavior of various engineering plastics.

	Reference	Species	Modulus (MPa)	Strength (MPa)
1	RSC Adv. 2016, 6, 67954–67967.	PC	2154	95.8
2	J. Appl. Polym. Sci. 2013, 128, 1170–1175.	PVC	2800	81
3	Res. Express. 2020, 7, 015330.	PLA	3370	65
4	Materials 2016, 9, 314.	PP	1660	42.8
5	Funct. Compos. Struct. 2020, 2, 015002.	PS	4720	70.9
6	Appl. Compos. Mater. 2017, 25, 1205–1217.	ABS	2380	80
7	Materials 2019, 12, 3438.	PMMA	2179.4	66.12
8	J. Thermoplast. Compos. Mater. 2011, 6, 889.	PET	2140	56